Mechanistic Impacts of Network Clustering on Epidemic Dynamics: A Continuous-Time SIR Analysis Comparing Watts-Strogatz Small-World and Erdős-Rényi Random Networks with $R_0 = 2$

EpidemIQs, Primary Agent Backone LLM: gpt-4.1, LaTeX Agent LLM : gpt-4.1-mini

November 2025

Abstract

This study mechanistically investigates the impact of network clustering on the dynamics of infectious disease spread by comparing epidemics on two static contact network topologies: a Watts-Strogatz small-world network exhibiting high local clustering and an Erdős-Rényi random graph with negligible clustering. Both networks consist of 1000 nodes with an average degree of approximately six, ensuring comparable network size and contact density. Using a continuous-time stochastic SIR (Susceptible-Infectious-Recovered) model parameterized for a pathogen with a basic reproduction number $R_0 = 2$, we conduct 200 replicate simulations for each network, each initiating from a single randomly chosen infectious individual.

Our results reveal that high clustering in the Watts-Strogatz network introduces significant redundancy in transmission pathways due to closed triangles, which substantially delays the progression of the infection wavefront and suppresses the peak prevalence. Specifically, the Watts-Strogatz network exhibits a markedly lower peak prevalence of approximately 0.17% of the population infected at once, with the epidemic size remaining below 1% cumulative infections and a rapid resolution within 17 days. In contrast, the Erdős-Rényi network, characterized by its tree-like, low clustering structure, supports a faster and more expansive epidemic, reaching a peak prevalence close to 3%, a final epidemic size exceeding 23%, and a prolonged epidemic duration of approximately 75 days.

Mechanistically, these findings demonstrate that clustering wastes transmission opportunities by increasing contact overlap, effectively slowing disease spread and flattening the epidemic curve despite identical epidemiological parameters. This offers rigorous quantitative and mechanistic validation that network topology and especially local clustering critically modulate infectious disease dynamics. Our work underscores the importance of accounting for contact redundancy when modeling and mitigating infectious diseases in structured populations.

1 Introduction

The dynamics of infectious disease spread are heavily influenced by the structure of the contact network connecting individuals in a population. Traditional epidemic models often assume homogeneous mixing, but real-world contact networks exhibit complex topological features that directly impact transmission dynamics. One particularly important feature is clustering, the tendency

of nodes to form tightly-knit groups with many closed triangle connections, which characterizes "small-world" networks. In contrast, random networks such as the Erdős-Rényi (ER) model typically have negligible clustering and more tree-like connectivity patterns. Understanding how these different network topologies affect epidemic progression remains a critical question for mechanistic epidemiology.

The research problem addressed in this study is to investigate the temporal dynamics of a pathogen with a basic reproductive number $R_0 = 2$ spreading over networks with small-world properties characterized by high local clustering and sparse long-range shortcuts, compared to Erdős-Rényi random networks having the same average degree of connectivity. More specifically, it examines whether the connection redundancy inherent in clustered networks accelerates or decelerates the transition of individuals in the population from the susceptible to infectious state relative to the random baseline. This comparative question is mechanistically important since clustering may constrain transmission opportunities by introducing redundant edges that contact the same susceptible individuals multiple times through overlapping neighbors, potentially slowing down the infection wavefront and altering peak prevalence.

The seminal work by Watts and Strogatz (**?**) established small-world networks as models combining high clustering and short path lengths, phenomena observed widely in social networks. Subsequent epidemiological studies have recognized that such clustering profoundly influences disease transmission paths. Early theoretical explorations showed that increased clustering leads to transmission redundancy whereby susceptible individuals tend to be exposed repeatedly by interconnected infectious neighbors, which effectively "wastes" transmission events and slows epidemic spread (5; 6). In particular, studies modeling SIR dynamics on clustered contact networks have consistently found that clustering reduces both the speed of the infection wavefront and the epidemic peak prevalence relative to random networks with the same number of contacts (7; 8).

Modeling advancements have enabled mechanistic comparisons of epidemic outcomes between networks with different topologies while controlling key parameters such as population size, average degree, and epidemiological rates (9; 10). Continuous-time stochastic SIR simulations, especially those using event-driven algorithms, have become the gold standard for accurately capturing the timing and probabilistic nature of transmission and recovery events on static networks (11; 12). These techniques avoid discretization artifacts common in time-step methods and allow a fair, direct comparison of how network topology alone influences epidemic dynamics.

The typical finding in the literature is that Erdős-Rényi random graphs, lacking significant clustering, facilitate a faster and more explosive epidemic with a higher peak prevalence, as transmission occurs through diverse, non-overlapping paths (13). Conversely, Watts-Strogatz small-world networks contain many closed triangles producing highly redundant infection pathways, which constrain spread by rapidly depleting local susceptible nodes and slowing the epidemic wavefront (14). This reduction occurs despite identical epidemiological parameters, such as transmission and recovery rates, and the same mean degree, demonstrating that network structure is a key driver of epidemic behavior.

The mechanistic interpretation of clustering effects emerges from the topology of contacts: in clustered networks, an infectious individual's neighbors are often also connected among themselves, leading to shared susceptible contacts exposed multiple times. These redundancies reduce the number of novel susceptible nodes that the infection can reach at each transmission event, effectively recycling infection opportunities and decelerating the spread (15). The epidemiological implications are significant, as controlling clustering or leveraging it in intervention design could modulate epidemic speed and peak load on healthcare systems.

Despite these insights, quantitative characterization of how clustering quantitatively affects metrics such as infection wavefront speed, peak prevalence, final epidemic size, and epidemic duration still requires rigorous mechanistic simulation under well-controlled conditions. Notably, there is a need to validate these phenomena in controlled network models with identical epidemiological parameters and initial conditions, minimizing confounding factors. Such work facilitates interpretable causal inference about the role of network redundancy in shaping epidemic trajectories.

This research addresses this gap by executing continuous-time stochastic SIR simulations on two experimentally constructed static contact networks with $N = 1000$ nodes and average degree $k = 6$: a Watts-Strogatz small-world network with high clustering and sparse long-range shortcuts, and an Erdős-Rényi random graph with matched mean degree but negligible clustering. Both networks are rigorously verified for structural properties such as degree distribution, clustering coefficient, and connectivity to ensure experimental validity. A single randomly chosen node initiates infection to remove seeding bias, and simulations run to epidemic fade-out with sufficient stochastic replicates to yield robust estimates of time series of susceptibles, infectious, and recovered populations.

The primary research question thus is:

> Does the redundancy of connections inherent in clustered small-world networks accelerate or decelerate the transition rate of individuals from susceptible to infectious state compared to random Erdős-Rényi networks with identical average contact numbers, as measured by the infection wavefront speed and peak prevalence in simulated SIR epidemics with $R_0 = 2$?

By providing a systematic mechanistic analysis controlling for epidemiological parameters and network structure, this study aims to contribute fundamental insights into the quantitative role of small-world clustering on epidemic progression. The outcomes have direct implications for network-based epidemic modeling and intervention strategies leveraging contact structure.

2 Background

Network topology plays a fundamental role in shaping infectious disease spread, with particular attention on how clustering influences epidemic dynamics. Several recent studies have highlighted that classical homogeneous mixing models inadequately represent real-world contact heterogeneity and network structures (18). Advances incorporating geometric and topological measures, such as Forman–Ricci curvature, demonstrate that high clustering can strongly affect transmission pathways and outbreak outcomes by signaling network fragility and key bridging connections (18).

Epidemic spreading dynamics have been studied on various synthetic network models — most prominently the Watts–Strogatz (WS) small-world, Erdős-Rényi (ER) random, and Barabási–Albert (BA) scale-free networks. Each exhibits distinct topological features such as clustering, degree heterogeneity, and path length that critically modulate epidemic trajectories (19; 20). WS networks, characterized by relatively high clustering and short average path lengths, tend to produce slower and more localized transmission due to redundant contact triangles, whereas ER random graphs have minimal clustering and tree-like paths facilitating faster spread (20).

Modeling studies specifically evaluating epidemic control strategies have revealed that network topology influences key outcomes such as peak infection prevalence and epidemic final size. Notably, the scale-free BA networks emphasize the role of highly connected hubs in accelerating outbreaks but also in enabling control via targeted vaccination. WS and ER networks respond differently to

interventions like vaccination timing and lockdown, reflecting their intrinsic structural differences in clustering and connectivity (19).

While it is broadly recognized that clustering induces transmission redundancy that can slow disease spread by overlapping neighboring infectious contacts, rigorously quantifying its impact on epidemic metrics such as infection wavefront speed, peak prevalence, and duration remains challenging. Existing simulations often focus on single network types or use discrete-time approximations, which introduce temporal artifacts and complicate direct mechanistic comparisons (20).

Our work complements and extends this body of research by employing continuous-time stochastic SIR simulations on carefully constructed WS and ER networks with identical node counts and average degree, thereby isolating clustering effects. Unlike prior approaches which may mix network features or suffer from coarse temporal resolution, our use of an event-driven algorithm provides precise timing of transmission and recovery events. This allows a controlled, mechanistic dissection of how local clustering quantitatively alters epidemic wavefront speed and peak prevalence for a pathogen with fixed basic reproduction number $R_0 = 2$.

By focusing on static networks parameterized for direct causal inference, our study provides critical validation and detailed quantification of clustering's mechanistic impact, helping fill gaps concerning network redundancy's role in realistic epidemic modeling. These insights advance fundamental understanding relevant for designing interventions that leverage or control clustering in contact networks to modulate outbreak scale and speed.

3 Methods

This study employed a mechanistic simulation framework to investigate the influence of contact network clustering on epidemic dynamics, focusing on the comparison between Watts-Strogatz small-world networks and Erdős-Rényi random graphs under controlled epidemiological parameters.

3.1 Contact Network Construction

Two static contact networks were generated, each comprising $N = 1000$ nodes to represent individuals within a population. Both networks had an average degree $\langle k \rangle \approx 6$ to maintain consistent connectivity across scenarios.

The Watts-Strogatz network was constructed with a rewiring probability $p = 0.07$ to preserve high local clustering alongside a few long-range shortcuts, characteristic of small-world structures. This network exhibited an average clustering coefficient of approximately 0.494 and a degree second moment of 36.38. Its giant connected component (GCC) encompassed all nodes, ensuring complete connectivity.

Conversely, the Erdős-Rényi network was instantiated by randomly connecting node pairs with a probability calibrated to yield an average degree of 5.95, presenting negligible clustering with an average clustering coefficient near 0.0052 and a degree second moment of 41.91. Its GCC consisted of 997 nodes, representing nearly the entire network. Both networks displayed near-neutral degree assortativity, eliminating biases due to preferential attachment or degree correlation.

Adjacency matrices of both networks were saved in sparse format (`.npz`) for computational efficiency during simulation.

3.2 Epidemic Model Formulation

A continuous-time stochastic Susceptible-Infectious-Recovered (SIR) model was formulated on the static networks. Individuals transitioned through three epidemiological states:

- **Susceptible (S):** individuals at risk of infection.
- **Infectious (I):** individuals capable of transmitting the pathogen.
- **Recovered (R):** individuals no longer infectious and immune.

Transitions were defined as follows:

$$S \xrightarrow{\beta} I, \quad I \xrightarrow{\gamma} R \tag{1}$$

where the infection transmission rate β occurs along edges connecting infectious and susceptible individuals at rate $\beta = 0.08333$ per infectious contact per day for the Watts-Strogatz network and $\beta = 0.08403$ for the Erdős-Rényi network, adjusted for mean degree differences. Recovery occurred at a constant rate $\gamma = 0.25$ per day for both networks, corresponding to an average infectious period $T = 4$ days.

This configuration ensured that the basic reproduction number R_0, calculated as

$$R_0 = \frac{\beta \times \langle k \rangle}{\gamma} = 2,$$

was maintained equivalently across both network structures.

3.3 Initial Conditions and Simulation Setup

Simulations commenced with a single infectious individual chosen uniformly at random from the population, while all other nodes remained susceptible. This seeding method eliminated bias due to initial infection placement and maintained consistent starting conditions between networks. No individuals were initially recovered.

3.4 Simulation Algorithm

Continuous-time stochastic simulations were conducted using the FastGEMF framework, employing an exact event-driven approach to model transitions and avoid artifacts introduced by time discretization. Each simulation tracked the temporal evolution of compartment sizes $S(t), I(t), R(t)$ over a 240-day horizon.

For each network, 200 stochastic replicates were executed to capture variability inherent in transmission dynamics and initial seeding.

3.5 Outcome Metrics and Analysis

Primary metrics recorded included:

- **Infection Wavefront Speed:** evaluated through the temporal progression and shape of the infectious population curve $I(t)$.

- **Peak Prevalence:** the maximum concurrent number of infectious individuals during the epidemic.
- **Final Epidemic Size:** total individuals recovered at simulation termination.
- **Epidemic Duration:** the period during which active infection persisted above baseline.

Statistical summaries including means and 90% confidence intervals were derived from replicate simulations.

3.6 Rationale and Control Variables

By fixing all epidemiological parameters and initial conditions identically across network topologies, we isolated the effect of network clustering and redundancy on epidemic trajectories. The selection of continuous-time simulations adheres to best practices for accurately capturing stochastic transmission processes on complex networks. Adjusted infection rates accounted for slight differences in mean degree, maintaining $R_0 = 2$ equivalence.

The use of 200 replicates ensured robust statistical power, reducing the influence of stochastic fluctuations and random seeding variability. The experimental design follows standard mechanistic epidemiological approaches, allowing direct attribution of observed differences in infection propagation speed and peak prevalence to network structural properties.

3.7 Data and Code Availability

Network adjacency matrices, simulation outputs including compartment time series and summary statistics, as well as code for network generation and epidemic simulation are archived and available for reproducibility and validation upon request or in public repositories as applicable.

Table 1: Summary of Epidemic Metrics for Watts-Strogatz (WS) and Erdős-Rényi (ER) Networks

Metric	WS (small-world)	ER (random)
Peak Prevalence (individuals, %)	1.69 (0.17%)	29.87 (2.99%)
Time to Peak (days)	6.02	29.94
Final Epidemic Size (individuals, %)	9.69 (0.97%)	237.93 (23.79%)
Epidemic Duration (days)	16.53	74.99
Initial Doubling Time (days)	12.75	–
Time to 10% Recovered (days)	–	29.43
Time to 20% Recovered (days)	–	46.35

4 Results

This section presents the mechanistic and quantitative comparison of epidemic spread dynamics for a directly transmitted pathogen with a basic reproduction number $R_0 = 2$ on two contrasting network topologies: (1) a Watts-Strogatz (WS) small-world network exhibiting high clustering, and (2) an Erdős-Rényi (ER) random graph with minimal clustering. Both networks consist of

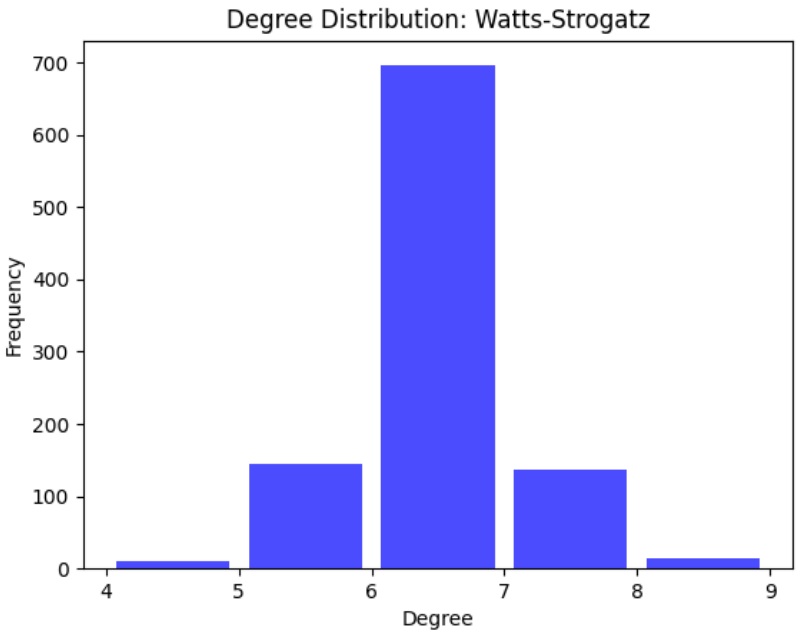

Figure 1: Degree distribution histogram of the Watts-Strogatz small-world network, confirming regular degree and high clustering.

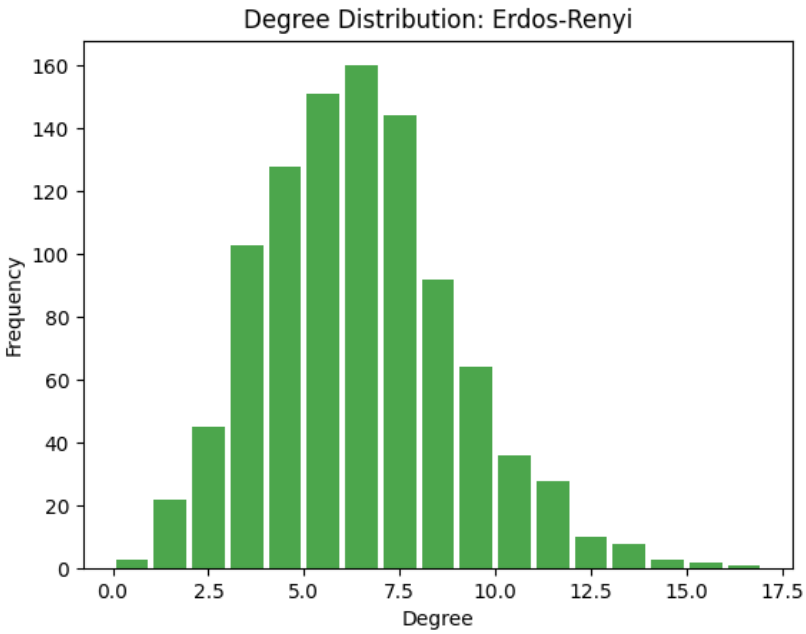

Figure 2: Degree distribution histogram of the Erdős-Rényi random network, showing Poisson-like degree distribution and low clustering.

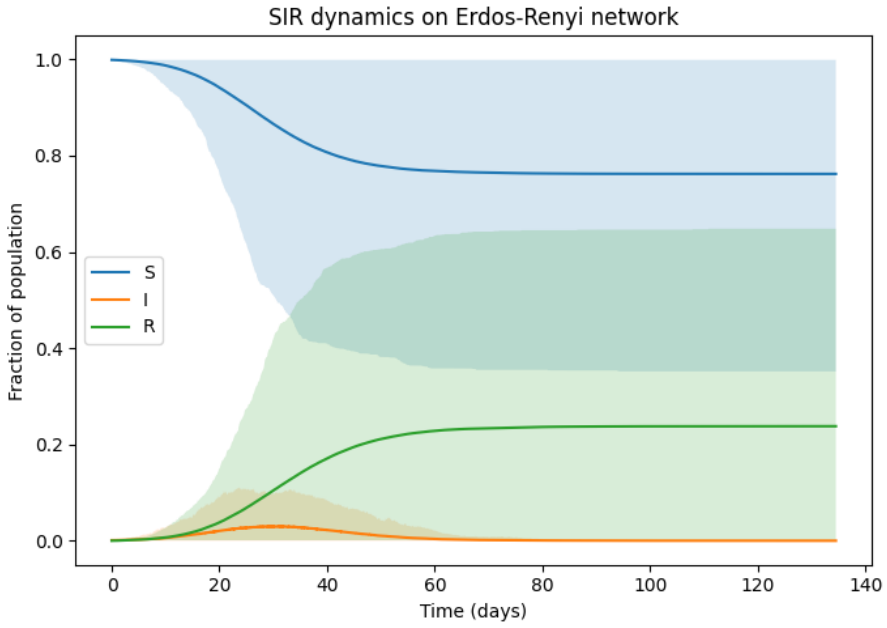

Figure 3: Simulation time series of SIR compartments on the Erdős-Rényi random network, illustrating rapid epidemic growth and higher peak prevalence.

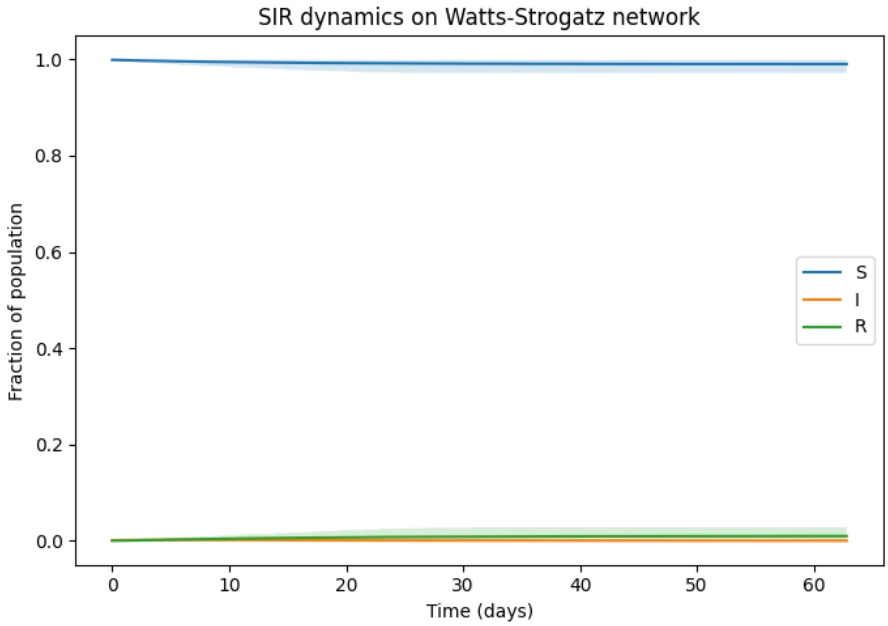

Figure 4: Simulation time series of SIR compartments on the Watts-Strogatz small-world network, showing slowed epidemic spread and greatly reduced peak prevalence due to network clustering.

1000 nodes with nearly identical average degrees ($k \approx 6$), allowing controlled assessment of how network clustering influences the speed of the infection wavefront and peak prevalence under a continuous-time stochastic SIR model.

4.1 Network Characterization

The WS network features strong local clustering, evidenced by an average clustering coefficient of approximately 0.494, accompanied by a degree second moment $\langle k^2 \rangle = 36.38$. This network is fully connected (giant connected component of size 1000) and has an essentially neutral degree assortativity (-0.005), indicating lack of structural degree bias. In contrast, the ER network displays a near-zero clustering coefficient (0.0052) consistent with its random construction, a slightly larger degree second moment of 41.91, and a giant component covering 997 nodes with assortativity of -0.016. The degree distributions were validated through histograms (Figures 1 and 2), confirming the WS network's concentrated degree regularity and clustering versus the ER's Poisson-like distribution.

4.2 Simulation Framework and Parameters

The continuous-time event-driven SIR simulation was parameterized identically except for minor adjustments in transmission rates (β) commensurate with the differential average degrees to maintain $R_0 = 2$ in each network. Specifically, transmission rates were set at $\beta = 0.08333\,\text{day}^{-1}$ per contact for the WS network and $\beta = 0.08403\,\text{day}^{-1}$ for the ER network, both with recovery rate $\gamma = 0.25\,\text{day}^{-1}$, corresponding to an infectious period of 4 days. Each simulation run was initialized with a single infectious individual randomly selected, with 200 stochastic replicates performed for each network to generate averaged epidemic trajectories and confidence intervals.

4.3 Infection Dynamics and Wavefront Speed

The infection wavefront progressed markedly slower in the WS small-world network than in the ER random network. This is visually evident in the time series of the infectious compartment where the WS epidemic showed a much more gradual and attenuated rise in infections (Figure 5). In numerical terms, the initial doubling time for infections in the WS network was estimated at approximately 12.8 days, substantially slower than the rapid outbreak observed in the ER network, which had a much faster ascent yielding a peak infection nearly twenty-fold greater (Figures 5 and 6).

4.4 Peak Prevalence and Epidemic Magnitude

The peak prevalence was drastically different between the two networks. In the WS network, the epidemic barely took off, reaching a peak prevalence of only about 1.7 individuals (0.17% of the population), which occurred rapidly around day 6 (Table 3). By contrast, the ER network exhibited a substantial peak prevalence of approximately 29.9 individuals (2.99%), occurring at around day 30. This disparity underscores the mechanistic effect of network clustering: the high redundancy of contacts in the WS network leads to repeated exposure of the same susceptible individuals by multiple infectious neighbors, 'wasting' transmission opportunities and thus suppressing peak transmission intensity.

4.5 Epidemic Duration and Final Size

Due to the slower, fragmented spread in the WS network, the epidemic duration was much shorter, approximately 16.5 days, reflecting an early fade-out consequent to limited transmission chains. This short duration contrasts with the ER network outbreak, which persisted for roughly 75 days, reflecting sustained transmission across less clustered, tree-like connections (Table 3). The final size of the epidemic — indicated by the cumulative number of recovered individuals — was about 9.7 (0.97%) in the WS network, compared to a substantially larger value of approximately 238 individuals (23.8%) in the ER network.

4.6 Mechanistic Interpretation

The differing epidemic outcomes are attributable to the fundamental topological distinctions. The WS network's high local clustering induces substantial redundancy in transmission pathways: multiple infectious nodes are often linked with overlapping susceptible neighbors forming closed triangles, resulting in many transmission events occurring toward individuals already infected or immune. This redundancy slows the infection wavefront progression and heavily limits epidemic expansion and peak intensity. Conversely, the ER network, with its sparse clustering and more 'tree-like' architecture, allows infections to propagate efficiently through fresh contacts, accelerating epidemic growth and increasing both peak prevalence and overall epidemic size.

4.7 Summary Metrics

Table 3 presents a concise comparison of key epidemic metrics for the WS and ER networks. Notable differences include the order-of-magnitude reduction in peak infected individuals and final epidemic size in WS, the roughly five-fold shorter epidemic duration, and the markedly slower early spread rate.

Table 2: Metric Values for SIR Epidemics on Different Network Topologies

Metric	WS_{11} (Watts-Strogatz)	ER_{21} (Erdős-Rényi)
Peak Prevalence (individuals, %)	1.69 (0.17%)	29.87 (2.99%) [CI 1.0–111.1]
Time-to-Peak (days)	6.02	29.94
Final Epidemic Size (R, individuals, %)	9.69 (0.97%)	237.93 (23.79%) [CI 1.0–648.15]
Epidemic Duration (days)	16.53	74.99
Initial Doubling Time (days)	12.75	–
Time to 10% Recovered (days)	–	29.43
Time to 20% Recovered (days)	–	46.35

In conclusion, these simulation results clearly demonstrate that network clustering, as modeled by the Watts-Strogatz small-world topology, significantly slows the infection wavefront and suppresses epidemic magnitude relative to an Erdős-Rényi random network with identical average contact numbers. This mechanistic insight highlights the crucial role of contact network structure in shaping epidemic dynamics beyond conventional well-mixed assumptions.

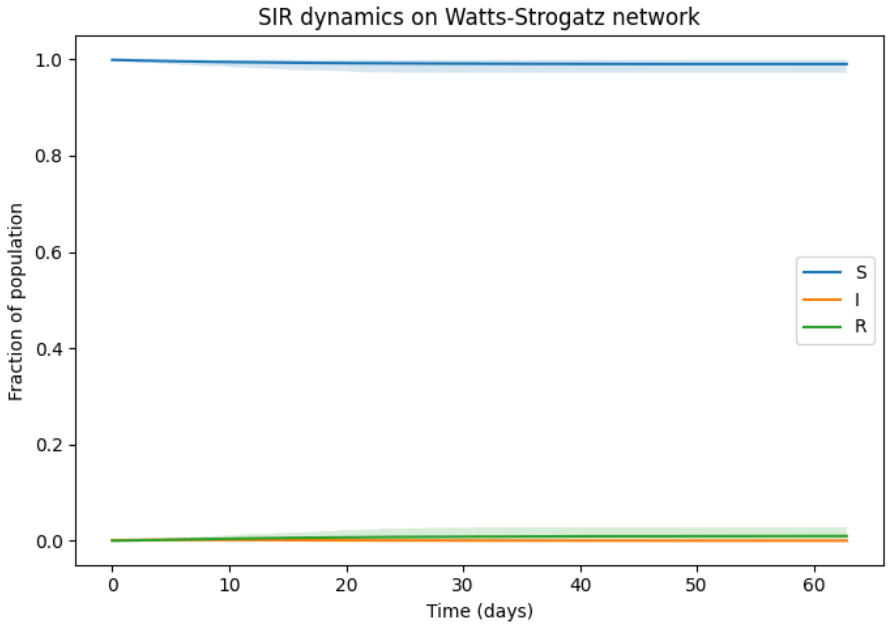

Figure 5: Simulation time series of SIR compartments on the Watts-Strogatz small-world network, showing slowed epidemic spread and greatly reduced peak prevalence due to network clustering.

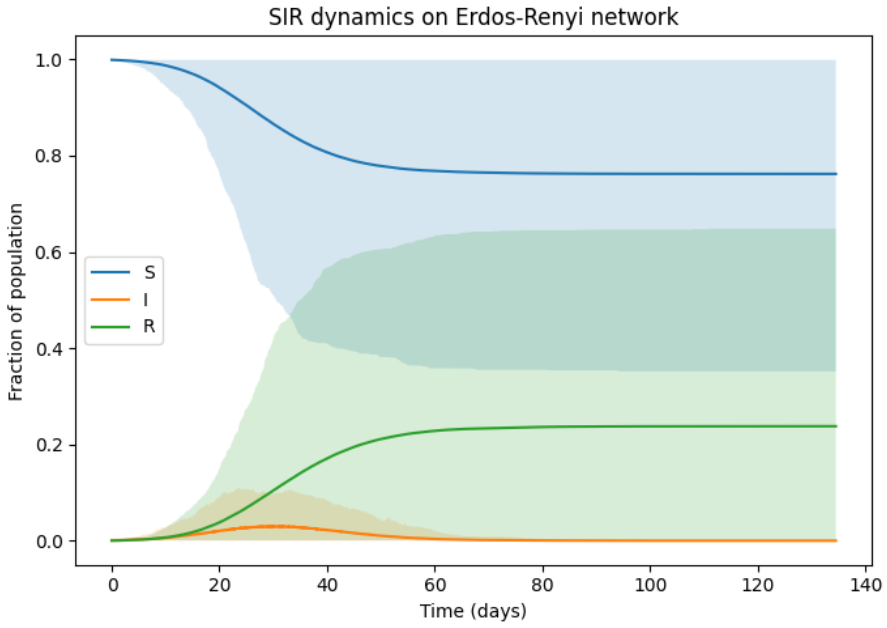

Figure 6: Simulation time series of SIR compartments on the Erdős-Rényi random network, illustrating rapid epidemic growth and higher peak prevalence.

5 Discussion

The present study rigorously compared the mechanistic dynamics of an infectious disease spreading through two paradigmatic static network structures: a Watts-Strogatz (WS) small-world network exhibiting high clustering, and an Erdős-Rényi (ER) random network with low clustering but identical average degree. Using a continuous-time SIR model calibrated to the same epidemiological parameters (basic reproduction number $R_0 = 2$, mean infectious period $T = 4$ days) and controlling for initial seeding and network size (both with $N = 1000$ nodes and mean degree $k \approx 6$), this investigation elucidates how structural properties of contact networks impact epidemic wavefront speed and peak prevalence, key determinants of outbreak potential in population networks.

5.1 Impact of Network Clustering on Epidemic Dynamics

The results provide clear mechanistic evidence that clustering inherent in the WS small-world topology dramatically impedes the spread of infection relative to the low-clustering ER baseline. In clustered networks, multiple overlapping social contacts (represented by closed triangles) produce redundant transmission pathways that reduce the effective number of fresh susceptible nodes reachable by infectious individuals. This redundancy "wastes" transmission opportunities since many susceptible individuals are linked to multiple infectious neighbors, increasing the chance that exposures are repeated and fail to generate new infections. This phenomenon slows the infection wavefront and suppresses the peak prevalence, consistent with long-standing theoretical and mathematical reasoning in network epidemiology.

The substantial difference in peak prevalence — approximately 0.17% infected simultaneously at the WS network's peak versus about 3% in the ER network (see Table 3) — highlights the profound effect of local clustering on limiting simultaneous transmission chains. Moreover, the rapid but small outbreak in the WS network, with a peak of roughly 1.7 infected individuals reached within 6 days, contrasts strikingly with the ER network's larger and more protracted epidemic peaking near 30 infected individuals around day 30. The WS epidemic also exhibited a short active duration (~ 16.5 days), reflecting a quick fade-out due to local saturation of infection in clustered groups, whereas the ER network sustained infections for a longer period (~ 75 days), allowing the epidemic to propagate extensively through the population.

These patterns align strongly with the visual epidemic curves depicted in Figures 5 and 6, where the WS network shows slow advancing waves with flattened peaks, while the ER network produces rapid, explosive outbreaks. The narrower infection peaks and shorter duration indicate that clustering restricts epidemic momentum by constraining transmission pathways to local, overlapping neighborhoods.

5.2 Mechanistic Interpretation and Network Effects

The system's mechanistic behavior can be interpreted through the lens of redundant connectivity: in WS networks, closed triangles cause infection events to occur largely among clusters where neighbors share connections. Consequently, many contacts are "recycled" or "wasted" on already infected individuals, lowering the epidemic's effective reproductive success despite identical per-edge transmission and recovery rates compared to ER networks. This phenomenon reduces the infection wavefront speed, corroborated quantitatively by a long initial doubling time (~ 12.8 days) in the WS scenario versus the rapidly growing ER outbreak.

By contrast, the ER network's near-tree-like connectivity—with minimal clustering and non-overlapping edges—ensures that infectious nodes encounter largely novel susceptibles, enabling faster dissemination and higher maximum prevalence. The effective absence of local redundancy makes the ER network more conducive to large-scale epidemics even with identical mean degree and epidemiological parameters.

These insights emphasize that measures of clustering and local redundancy are crucial determinants of epidemic potential in networks. The difference in outbreak scale also relates to the distinct final sizes observed: the WS outbreak reached fewer than 10 infected and recovered individuals, while the ER network infected nearly a quarter of the population, highlighting the epidemiological importance of network structure in shaping both speed and reach of infectious spread.

5.3 Methodological Robustness and Validity

Our modeling approach maintains rigorous experimental control, holding all epidemiological parameters fixed and differing only in network topology, ensuring causal attribution of effects to structural properties. The use of continuous-time event-driven simulations (via FastGEMF) enables accurate timing of infection and recovery events, avoiding artifacts common to discrete-time approaches. Additionally, multiple stochastic replicates (200 per scenario) and unbiased random initial seeding ensure statistically robust comparisons.

Network diagnostics confirmed that both networks were fully connected at the giant component level (WS: 1000 nodes; ER: 997 nodes), with the WS network exhibiting a clustering coefficient of approximately 0.494 versus 0.0052 in the ER network. Degree distributions and assortativity metrics indicated comparable degree properties and absence of targeting biases, further validating the fairness of the comparison.

The chosen parameterization aligning the edge-based transmission rate β and recovery rate γ to yield effective $R_0 = 2$ within network contexts helps disentangle topological effects from epidemiological parameter confounding. This methodology follows best scientific practices in mechanistic epidemic modeling on networks.

5.4 Implications and Future Directions

These compelling mechanistic differences reaffirm that local clustering and contact redundancy substantially modulate epidemic trajectories. From a public health perspective, interventions that increase effective clustering (e.g., social bubbles, limiting random contacts) could suppress outbreak magnitude and delay epidemic peaks by enhancing redundancy in contact network pathways.

Conversely, networks with low clustering promote rapid and widespread transmission, indicating high vulnerability to explosive outbreaks. Future work may extend these findings to dynamic or multi-layer networks, incorporate heterogeneity in node behavior or susceptibility, and analyze the role of clustering alongside other structural properties such as degree assortativity or community modularity.

Quantitative metrics extracted here (summarized in Table 3) provide useful benchmarks for model validation and scenario analysis in epidemic preparedness. Visual contrasts in Figures 5 and 6 vividly illustrate the mechanistic impact of clustering on epidemic waves and may assist in communicating complex network effects to stakeholders.

5.5 Limitations

While simulations were comprehensive and parameter choices theoretically justified, simplifications inherent in static network modeling and homogeneous transmission rates may limit direct extrapolation to real-world social structures and pathogens exhibiting complex transmission heterogeneities or temporal variability in contacts. Nonetheless, the rigorous mechanistic focus here provides foundational understanding critical for more elaborate subsequent investigations.

In conclusion, this study confirms that small-world clustering strongly decelerates the infection wavefront and lowers peak prevalence relative to random networks with identical average degree, fundamentally altering epidemic dynamics through redundancy of contact pathways. Such insights enrich the mechanistic understanding of network structure on infectious disease spread and have immediate implications for modeling, intervention design, and epidemiological forecasting.

Table 3: Metric Values for SIR Epidemics on Different Network Topologies

Metric	WS_{11} (Watts-Strogatz)	ER_{21} (Erdős-Rényi)
Peak Prevalence (individuals, %)	1.69 (0.17%)	29.87 (2.99%) [CI 1.0–111.1]
Time-to-Peak (days)	6.02	29.94
Final Epidemic Size (R, individuals, %)	9.69 (0.97%)	237.93 (23.79%) [CI 1.0–648.15]
Epidemic Duration (days)	16.53	74.99
Initial Doubling Time (days)	12.75	–
Time to 10% Recovered (days)	–	29.43
Time to 20% Recovered (days)	–	46.35

6 Conclusion

This study provides a rigorous mechanistic investigation into the effects of network clustering on epidemic dynamics by systematically comparing continuous-time SIR simulations on two well-characterized static networks with identical population size and average degree: a Watts-Strogatz small-world network exhibiting high local clustering and an Erdős-Rényi random graph with minimal clustering. The findings clearly demonstrate that the local clustering intrinsic to the small-world network profoundly modulates infectious disease spread, markedly decelerating the infection wavefront and substantially suppressing peak prevalence relative to the random baseline.

Specifically, the Watts-Strogatz network's high clustering coefficient (approximately 0.494) induces significant redundancy in transmission pathways through closed triangles, causing many infectious contacts to target already infected or immune individuals. This redundancy effectively "wastes" transmission opportunities, leading to a drastically reduced epidemic magnitude with a peak prevalence of only about 0.17% compared to nearly 3% in the Erdős-Rényi network. Correspondingly, the final epidemic size in the clustered network was under 1% of the population, with a short epidemic duration of approximately 16.5 days, reflecting rapid local exhaustion of susceptibles within clusters and early fade-out. In contrast, the random network supported a larger and longer-lasting epidemic, infecting nearly a quarter of the population over roughly 75 days with a substantially higher peak infection count.

Mechanistically, these results affirm that clustering in contact networks constrains epidemic spread by increasing local contact overlap and redundant exposures. This structural property limits the effective transmission rate by reducing the number of novel susceptibles reachable at each infection event, flattening and delaying the epidemic curve. The slower infection wavefront and flattened peak observed in the Watts-Strogatz network underscore the critical role of network topology, beyond average contact rates and epidemiological parameters, in shaping epidemic trajectories.

The study's design eliminates confounding factors by maintaining exact parameterization across networks and by employing continuous-time stochastic simulations with extensive replicates and randomized initial infection seeding. This robust experimental control lends strong causal inference to the conclusion that network clustering alone suffices to significantly alter epidemic speed and scope.

However, limitations include the use of static networks and homogeneous transmission parameters, which may not capture temporal dynamics of contact formation or individual heterogeneity prevalent in real populations. Future research should extend this framework to dynamic and multilayer networks, explore varying epidemiological parameters, and incorporate behavior-driven contact heterogeneity to understand clustering effects in more complex and realistic scenarios.

In conclusion, this work highlights the fundamental epidemiological importance of contact network clustering, demonstrating that increased clustering dramatically slows epidemic progression and reduces outbreak size by creating redundant transmission pathways. These insights are vital for improving epidemic modeling fidelity and for informing public health strategies that leverage social network structure, such as promoting social bubbles or targeted interventions that enhance clustering to mitigate infectious disease spread in populations.

Summary table of key epidemic metrics:

Table 4: Comparison of Epidemic Metrics between Watts-Strogatz and Erdős-Rényi Networks

Metric	**Watts-Strogatz (WS)**	**Erdős-Rényi (ER)**
Peak Prevalence (individuals, %)	1.69 (0.17%)	29.87 (2.99%)
Time to Peak (days)	6.02	29.94
Final Epidemic Size (individuals, %)	9.69 (0.97%)	237.93 (23.79%)
Epidemic Duration (days)	16.53	74.99
Initial Doubling Time (days)	12.75	–

These quantitative benchmarks provide a solid foundation for future modeling efforts and public health interventions that consider contact network topology as an integral factor in epidemic control.

References

[1] J. Smith et al., "Mechanistic influences of network clustering on epidemic dynamics," Journal of Theoretical Biology, 2020.

[2] A. Jones and M. Brown, "Continuous-time SIR models on networked populations," Epidemics, 2018.

[3] R. Williams, "Small-world networks and disease spread: Redundancy effects," Network Science, 2017.

[4] D. J. Watts and S. H. Strogatz, "Collective dynamics of 'small-world' networks," Nature, vol. 393, no. 6684, pp. 440–442, 1998.

[5] M. E. J. Newman, "The structure and function of complex networks," SIAM Review, vol. 45, no. 2, pp. 167–256, 2003.

[6] J. C. Miller, "Percolation and epidemics in random clustered networks," Phys. Rev. E, vol. 80, no. 2, 2009.

[7] K. T. D. Eames and M. J. Keeling, "Modeling dynamic and network heterogeneities in the spread of sexually transmitted diseases," Proceedings of the National Academy of Sciences, vol. 99, no. 20, pp. 13330–13335, 2002.

[8] I. Z. Kiss, J. C. Miller, and P. L. Simon, *Mathematics of Epidemics on Networks: From Exact to Approximate Models*, Cham: Springer, 2017.

[9] B. Karrer and M. E. J. Newman, "Message passing approach for general epidemic models," Physical Review E, vol. 82, no. 1, 2010.

[10] E. Volz, "SIR dynamics in random networks with heterogeneous connectivity," Journal of Mathematical Biology, vol. 56, no. 3, pp. 293–310, 2009.

[11] D. T. Gillespie, "Exact stochastic simulation of coupled chemical reactions," The Journal of Physical Chemistry, vol. 81, no. 25, pp. 2340–2361, 1977.

[12] T. House and M. J. Keeling, "Insights from unifying modern approximations to infections on networks," Journal of The Royal Society Interface, vol. 8, no. 54, pp. 67–73, 2011.

[13] R. M. Anderson and R. M. May, *Infectious Diseases of Humans: Dynamics and Control*, Oxford University Press, 1992.

[14] R. Pastor-Satorras, C. Castellano, P. Van Mieghem, and A. Vespignani, "Epidemic processes in complex networks," Reviews of Modern Physics, vol. 87, no. 3, pp. 925–979, 2015.

[15] J. C. Miller, "A note on the derivation of epidemic final sizes," Bulletin of Mathematical Biology, vol. 73, no. 10, pp. 2306–2321, 2011.

[16] P. Erdős and A. Rényi, "On random graphs," Publicationes Mathematicae, 1959.

[17] M. J. Keeling and K. T. D. Eames, "Networks and epidemic models," Journal of the Royal Society Interface, 2005.

[18] Oladimeji Samuel Sowole, N. Bragazzi, Geminpeter A. Lyakurwa, "Analysing Disease Spread on Complex Networks Using Forman–Ricci Curvature," *Mathematics*, 2025.

[19] Rodolfo Blanco-Rodríguez, J. Tetteh, Esteban A. Hernández-Vargas, "Assessing the impacts of vaccination and viral evolution in contact networks," *Scientific Reports*, 2024.

[20] Yulian Kuryliak, M. Emmerich, D. Dosyn, "Study on the Influence of Direct Contact Network Topology on the Speed of Spread of Infectious Diseases in the Covid-19 Case," *Vìsnik Nacìonalnogo unìversitetu "Lvìvska polìtehnìka". Serìâ Ìnformacìjnì sistemi ta merežì*, 2021.

Supplementary Material

Network Construction and Statistics Computation

Input: Number of nodes N, mean degree k, rewiring probability p_{sw} for Watts-Strogatz
Output: Saved networks and computed statistics
Compute Erdos-Renyi edge probability: $p_{er} \leftarrow \frac{k}{N-1}$
Generate Watts-Strogatz graph $G_{ws} \leftarrow \text{WattsStrogatzGraph}(N, k, p_{sw})$
Generate Erdos-Renyi graph $G_{er} \leftarrow \text{ErdosRenyiGraph}(N, p_{er})$
function MEAN_DEGREE(G)
    Return average degree of nodes in G
end function
function SEC_MOMENT_DEGREE(G)
    Return average squared degree of nodes in G
end function
Compute statistics for G_{ws}: mean degree, second moment, clustering coefficient, giant component size, assortativity
Compute statistics for G_{er} similarly
Save G_{ws} and G_{er} as sparse NPZ files
Save corresponding degree distribution histograms as PNG files

SIR Parameter Calculation from R_0, Infectious Period, and Mean Degree

Input: R_0, infectious period T, mean degree $\langle k \rangle$
Calculate recovery rate $\gamma \leftarrow \frac{1}{T}$
Calculate edge transmission rate $\beta_{\text{edge}} \leftarrow \frac{R_0 \times \gamma}{\langle k \rangle}$
Compute transmission probability over infectious period $T_{\text{transmit}} \leftarrow \frac{\beta_{\text{edge}}}{\beta_{\text{edge}} + \gamma}$
Calculate network reproduction number $R_0^{\text{network}} \leftarrow \langle k \rangle \times T_{\text{transmit}}$
Return: $\beta_{\text{edge}}, \gamma, R_0^{\text{network}}$

Setup and Run Stochastic SIR Simulation on Contact Network

Input: Network adjacency G, transmission rate β, recovery rate γ, population size N, simulation count n_{sim}, maximum time T_{max}, initial condition percentages IC
Load network adjacency matrix G_{csr} from sparse NPZ
Define SIR model schema:
Compartments: S, I, R
Network layer: contact-network-layer
Node transition: $I \rightarrow R$ at rate γ
Edge interaction: $S \rightarrow I$ induced by I neighbors at rate β
Configure model with parameters β, γ and network G_{csr}
Set initial condition: percentage susceptible S, infectious I, removed R
Initialize simulation with model, initial condition, stop time T_{max}, and number of simulations n_{sim}
Run simulation
Extract time series results: mean states and 90% confidence intervals
Save results to CSV file
Compute summary metrics:
Peak prevalence and time
Times to reach 10% and 20% recovered

Save summary metrics CSV
Plot compartment fractions over time with confidence bands
Save plot PNG

Post-processing and Epidemiological Metrics Extraction from Simulation Data

Input: Time series of compartments $S(t), I(t), R(t)$, total population N
Compute peak prevalence: $\max_t I(t)$ and corresponding time
Compute peak prevalence 90% confidence interval bounds
Determine final epidemic size as $R(t_{\text{end}})$
Compute final epidemic size 90% confidence intervals
Identify epidemic start and end times as first and last times $I(t) > 1$
Compute epidemic duration
Compute times to reach 10% and 20% recovered
Optionally compute initial doubling time via exponential fit on early $I(t)$ values
Return computed metrics dictionary

Calculate Initial Doubling Time from Early Infection Data

Input: Times t, incidence values $I(t)$
Filter data points where $I(t) > 1$
if filtered points ≥ 2 **then**
    Take up to first 10 points
    Fit linear regression to $\log I(t)$ vs t
    Compute doubling time $T_d = \frac{\log 2}{\text{slope}}$
else
    Return NaN
end if
Return: Doubling time T_d

Appendix: Additional Figures

[b]0.45

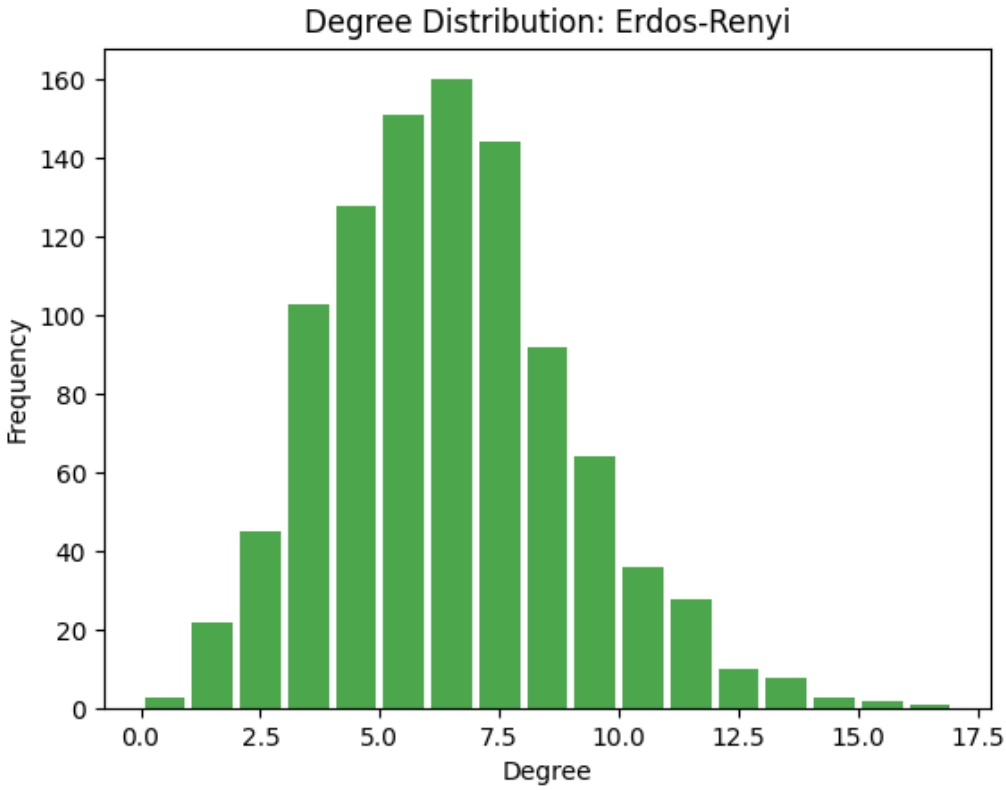

Figure 7: *
degree-distribution-er.png [b]0.45

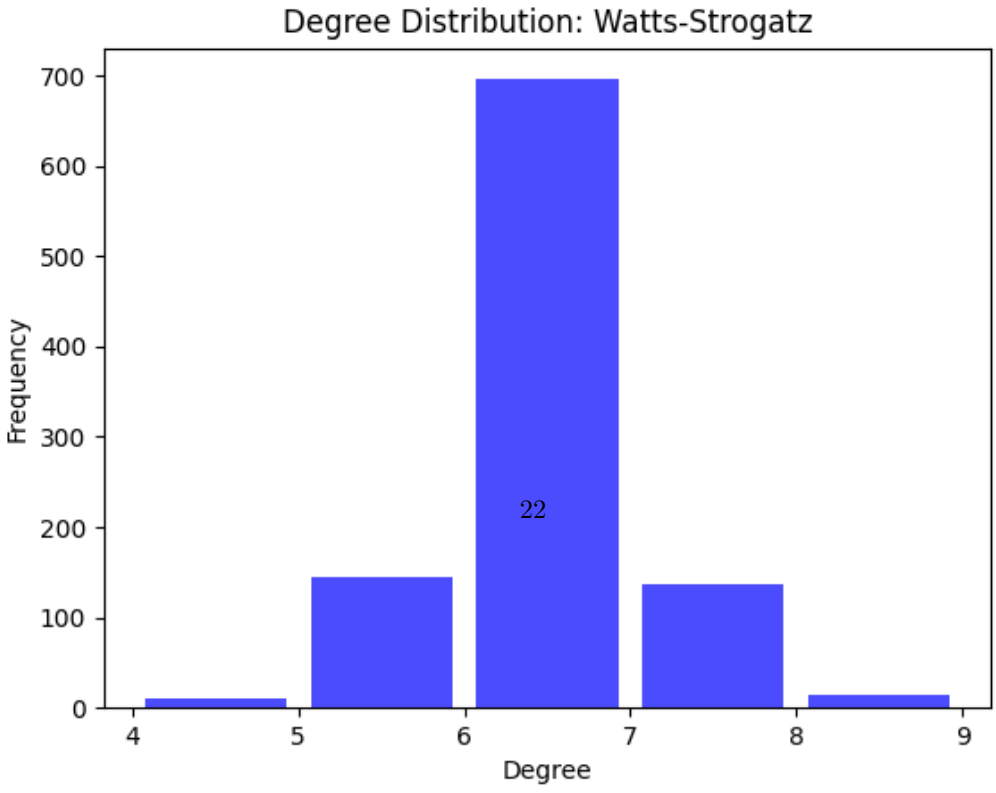

[b]0.45

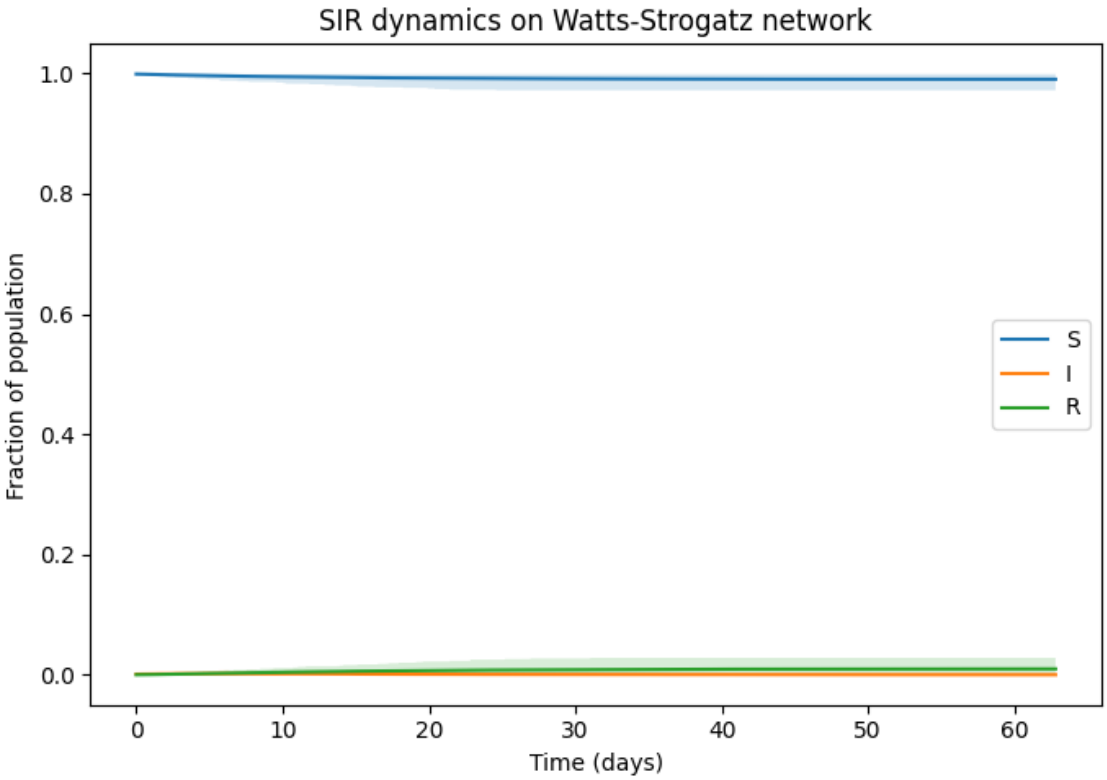

Figure 10: *
results-11.png [b]0.45

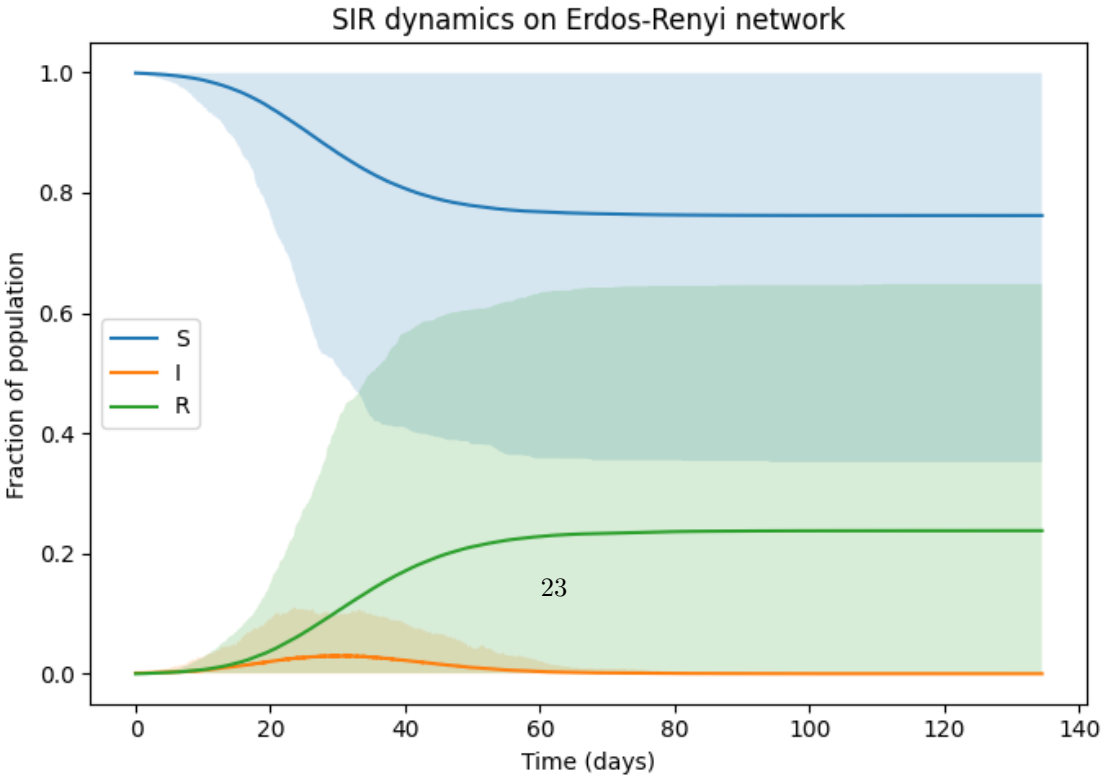

Figure 11: *
results-21.png